polyketide intermediates constructed by the highly conserved warhead PKS. This remarkable CalE8/SgcE relationship establishes a new paradigm for the enediyne PKS, distinct from other known bacterial type I interative PKSs and opens the door for bioengineering novel enediyne variants.

References and Notes

1. J. S. Thorson *et al*., *Curr. Pharm. Des.* **6**, 1841 (2000).
2. N. Zein, A. M. Sinha, W. J. McGaharen, G. A. Ellestad, *Science* **240**, 1198 (1988).
3. A. G. Myers, S. B. Cohen, B. M. Kwon, *J. Am. Chem. Soc.* **116**, 1255 (1994).
4. J. J. DeVoss, J. J. Hangeland, C. A. Townsend, *J. Am. Chem. Soc.* **112**, 4554 (1990).
5. C. M. H. Watanabe, L. Supekova, P. G. Schultz, *Chem. Biol.* **9**, 245 (2002).
6. E. L. Sievers, M. Linenberger, *Curr. Opin. Oncol.* **13**, 522 (2001).
7. S. J. Danishefsky, M. D. Shair, *J. Org. Chem.* **61**, 16 (1996).
8. K. S. Lam *et al*., *J. Am. Chem. Soc.* **115**, 12340 (1993).
9. W. Liu, S. D. Christenson, S. Standage, B. Shen, *Science* **247**, 1170 (2002).
10. O. D. Hensens, J.-L. Giner, I. H. Goldberg, *J. Am. Chem. Soc.* **111**, 3295 (1989).
11. R. W. Whitwam, J. Ahlert, T. R. Holman, M. Ruppen, J. S. Thorson, *J. Am. Chem. Soc.* **122**, 1556 (2000).
12. Most likely owing to the toxic nature of some of the gene products when cloned into *Escherichia coli* (J. Ahlert *et al*., unpublished observations).
13. The sequence is submitted under GenBank Accession numbers AF505622 and AF497482.
14. G. Weitnauer *et al*., *Chem. Biol.* 8, 569 (2001).
15. H. Takeyama, D. Takeda, K. Yazawa, A. Yamada, T. Matsunaga, *Microbiology* **143**, 2725 (1997).
16. N. Morita, M. Tanaka, H. Okuyama, *Biochem. Soc. Trans.* **28**, 943 (2000).
17. J. G. Metz *et al*., *Science* **293**, 290 (2001).
18. S. F. Love, W. M. Maiese, D. M. Rothstein, *Appl. Environ. Microbiol.* **58**, 1376 (1992).
19. Strain LL6000 is an optimized production strain provided by Wyeth Research which, under typical growth conditions, provides ~0.8 mg/liter of the calicheamicins.
20. M. Greenstein, T. Monji, R. Yeung, W. M. Maiese, R. J. White, *Antimicrob. Agents Chemother.* **29**, 861 (1986).
21. J. B. Biggins, J. R. Prudent, D. J. Marshall, M. Ruppen, J. S. Thorson, *Proc. Natl. Acad. Sci. U.S.A.* **97**, 13537 (2000).
22. Using the HPLC conditions described in the supporting material on *Science* Online, the namenamicin standard has a retention time of 18.3 min. This compound also displays strong activity in both the BIA (biochemical lambda prophage induction) and the MBL ("molecular break lights") assays (J. B. Biggins, unpublished data).
23. J. Staunton, K. J. Weissman, *Nat. Prod. Rep.* **18**, 380 (2001).
24. M. Bierman *et al*., *Gene* **116**, 43 (1992).
25. J. Ahlert *et al*., unpublished observations.

26. We gratefully acknowledge Wyeth Research for graciously providing materials and P. R. Hamann for helpful discussion. J.S.T. is a Rita Allen Foundation Scholar and Alfred P. Sloan Fellow. This work was supported in part by grants from the National Institutes of Health (CA84374 and GM58196), the Mizutani Foundation for Glycoscience, and a Cancer Center Support Grant (CA08748). We also thank the Charles A. Dana and Norman and Rosita Winston Foundations for postdoctoral fellowship support (J.A. and R.E.W.).

Supporting Online Material
www.sciencemag.org/cgi/content/full/297/5584/1173/DC1
Materials and Methods
Fig. S1

21 March 2002; accepted 10 June 2002

Structures of Glycoprotein Ibα and Its Complex with von Willebrand Factor A1 Domain

Eric G. Huizinga,[1]*† Shizuko Tsuji,[2]* Roland A. P. Romijn,[2] Marion E. Schiphorst,[2] Philip G. de Groot,[2] Jan J. Sixma,[2] Piet Gros[1]†

Transient interactions of platelet-receptor glycoprotein Ibα (GpIbα) and the plasma protein von Willebrand factor (VWF) reduce platelet velocity at sites of vascular damage and play a role in haemostasis and thrombosis. Here we present structures of the GpIbα amino-terminal domain and its complex with the VWF domain A1. In the complex, GpIbα wraps around one side of A1, providing two contact areas bridged by an area of solvated charge interaction. The structures explain the effects of gain-of-function mutations related to bleeding disorders and provide a model for shear-induced activation. These detailed insights into the initial interactions in platelet adhesion are relevant to the development of antithrombotic drugs.

Transient interactions of platelet-receptor glycoprotein Ibα (GpIbα) and immobilized von Willebrand factor (VWF) mediate the rolling of platelets at sites of vascular damage. Rolling reduces platelet velocity and prolongs the contact time with reactive components of the cell matrix. This facilitates platelet activation and subsequent integrin-mediated firm attachment (*1*). Platelet GpIbα and VWF coexist in the circulation but do not interact at a detectable level unless shear stress is applied or exogenous modulators like the snake venom botrocetin are added (*2*). Four types of congenital bleeding disorders have been defined that are caused by mutations in GpIbα or VWF, either enhancing or reducing complex formation. Shear-induced GpIbα-VWF interaction in occluded atherosclerotic arteries or at the surface of ruptured atherosclerotic plaques contributes critically to the onset of arterial thrombosis (*3*).

GpIbα is the central component of a receptor complex consisting of glycoproteins Ibα and Ibβ, IX, and V. It anchors the complex to the cytoskeleton and harbors the VWF-binding function in its ~290 NH_2-terminal residues. The VWF-binding site is exposed well above the platelet surface, being connected to a ~45-nm-long highly O-glycosylated stalk (*4*). The ~250-kD VWF protein forms large disulfide-bonded multimers with molecular sizes of up to 10 MD. It is found in plasma and the subendothelial cell matrix and is released from storage granules when platelets and endothelial cells are activated. A VWF multimer acts as the bridging ligand between platelets and the cell matrix through collagen binding by its A3 domain and through GpIbα binding by its A1 domain (*5*).

Although the crystal structure of VWF-A1 is known (*6*, *7*) and there is a large body of mutagenesis data (*8*–*15*), the precise interactions between GpIbα and A1, the mechanism of shear-induced activation, and the molecular basis of related bleeding disorders are poorly understood. We present crystal structures of the NH_2-terminal domain of GpIbα (residues 1 to 290) and its complex with the VWF-A1 domain (residues 498 to 705; VWF residue numbering used here starts at the first residue of the mature subunit, and the addition of 763 converts the numbering to that of preproVWF) (Table 1). We expressed recombinant GpIbα with the mutations N21Q and N159Q to remove N-glycosylation sites (*16*). Crystallization of the complex required the use of gain-of-function mutants GpIbα-M239V and A1-R543Q, which are associated with platelet-type and type 2B von Willebrand diseases and cause an enhanced affinity for complex formation [dissociation constant (K_d) = 5.8 nM (*16*)].

The crystal structure of the VWF-binding domain of GpIbα displays an elongated, curved shape (Fig. 1A) that is typical for proteins containing leucine-rich repeats (*17*). Eight short leucine-rich repeats, seven of which were predicted on the basis of the amino acid sequence, make up the central region of the molecule. Flanking sequences, which are conserved among numerous extracellular proteins including the other members of the GpIb-IX-V com-

[1]Department of Crystal and Structural Chemistry, Bijvoet Center for Biomolecular Research, Utrecht University, Padualaan 8, 3584 CH Utrecht, Netherlands. [2]Thrombosis and Haemostasis Laboratory, Department of Haematology, Institute of Biomembranes, University Medical Center Utrecht, Netherlands.

*These authors contributed equally to this work.
†To whom correspondence should be addressed. E-mail: e.g.huizinga@chem.uu.nl (E.G.H.), p.gros@chem.uu.nl (P.G.)

plex, cap the leucine-rich repeats. The NH_2-terminal sequence forms a 14-residue β hairpin delimited by a conserved disulfide bond between Cys^4 and Cys^{17}. The tip of the β hairpin, which we refer to as the β finger, protrudes from the protein surface and is disordered in one of the two molecules in the asymmetric unit. The COOH-terminal sequence, up to residue 267, contains a nine-residue α helix and four short 3_{10} helices. The anionic region beyond residue 267 was not visible in the electron density and was not modeled. Conserved disulfide bonds between Cys^{209} and Cys^{248} and between Cys^{211} and Cys^{264} stabilize the irregular fold of the COOH-terminal region. Residues 227 to 241

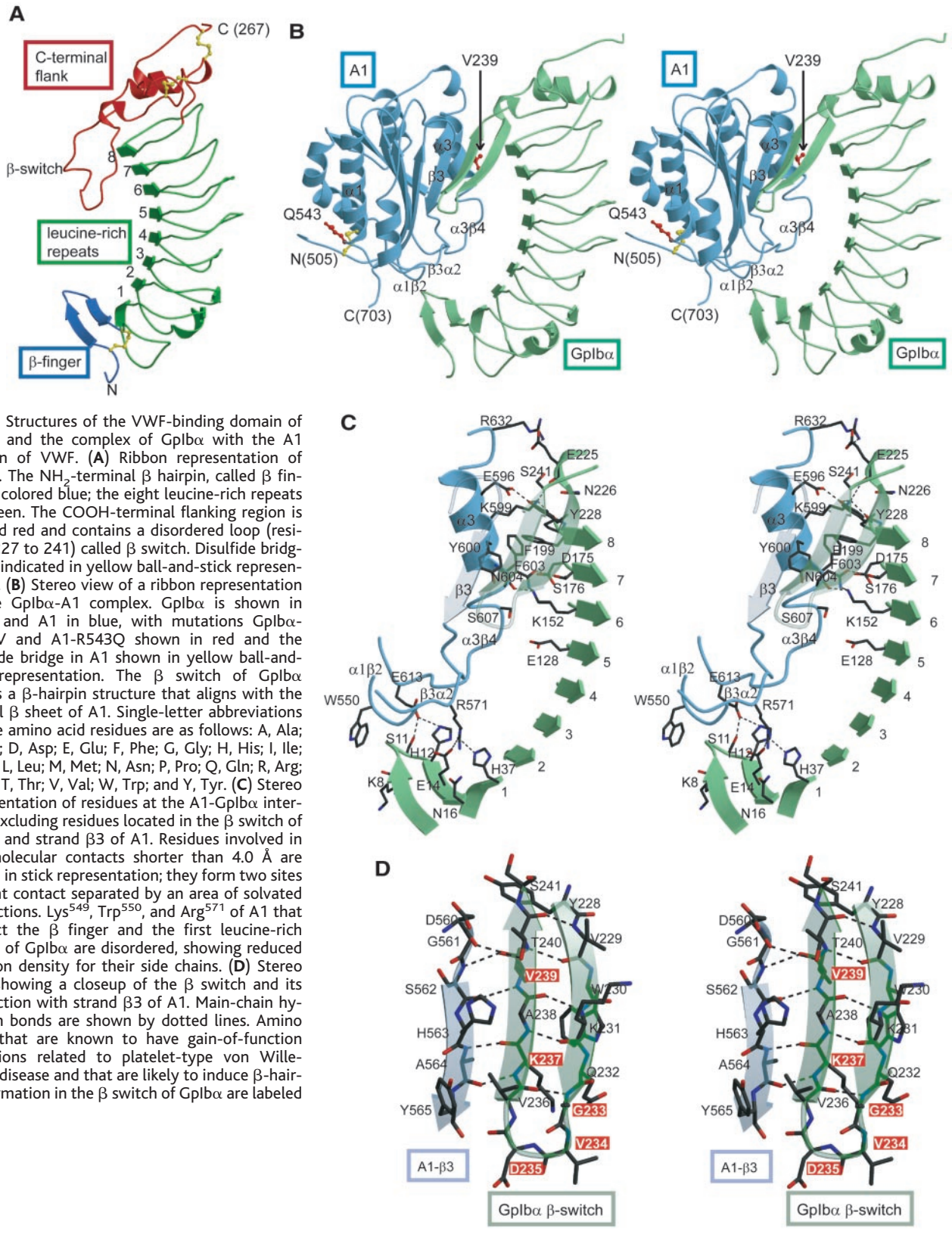

Fig. 1. Structures of the VWF-binding domain of GpIbα and the complex of GpIbα with the A1 domain of VWF. (**A**) Ribbon representation of GpIbα. The NH_2-terminal β hairpin, called β finger, is colored blue; the eight leucine-rich repeats are green. The COOH-terminal flanking region is colored red and contains a disordered loop (residues 227 to 241) called β switch. Disulfide bridges are indicated in yellow ball-and-stick representation. (**B**) Stereo view of a ribbon representation of the GpIbα-A1 complex. GpIbα is shown in green and A1 in blue, with mutations GpIbα-M239V and A1-R543Q shown in red and the disulfide bridge in A1 shown in yellow ball-and-stick representation. The β switch of GpIbα adopts a β-hairpin structure that aligns with the central β sheet of A1. Single-letter abbreviations for the amino acid residues are as follows: A, Ala; C, Cys; D, Asp; E, Glu; F, Phe; G, Gly; H, His; I, Ile; K, Lys; L, Leu; M, Met; N, Asn; P, Pro; Q, Gln; R, Arg; S, Ser; T, Thr; V, Val; W, Trp; and Y, Tyr. (**C**) Stereo representation of residues at the A1-GpIbα interface, excluding residues located in the β switch of GpIbα and strand β3 of A1. Residues involved in intermolecular contacts shorter than 4.0 Å are shown in stick representation; they form two sites of tight contact separated by an area of solvated interactions. Lys^{549}, Trp^{550}, and Arg^{571} of A1 that contact the β finger and the first leucine-rich repeat of GpIbα are disordered, showing reduced electron density for their side chains. (**D**) Stereo view showing a closeup of the β switch and its interaction with strand β3 of A1. Main-chain hydrogen bonds are shown by dotted lines. Amino acids that are known to have gain-of-function mutations related to platelet-type von Willebrand disease and that are likely to induce β-hairpin formation in the β switch of GpIbα are labeled in red.

project from the concave face of the molecule, forming a highly flexible loop that shows disorder in both molecules in the asymmetric unit. A sequence alignment of COOH-terminal–flanking regions (*18*) showed that the protruding loop is not a conserved feature in this domain family.

The crystal structure of the complex GpIbα–VWF-A1 shows that the globular A1 domain interacts with the concave face of GpIbα (Fig. 1B). The interaction surface is extended but discontinuous, comprising two distinct areas of tight interactions (Fig. 1C). The first and most extensive contact site is located near the top of A1 and buries a solvent-accessible surface of ~1700 Å^2. At this contact site, leucine-rich repeats 5 to 8 and the COOH-terminal flank of GpIbα interact with A1 helix α3, loop α3β4, and strand β3 (Fig. 1, C and D). The second and smaller contact site buries a surface of ~900 Å^2 and involves interactions of the NH_2-terminal β finger and the first leucine-rich repeat of GpIbα with loops α1β2, β3α2, and α3β4 at the bottom face of the A1 domain. As for the native structure of GpIbα, we did not observe the electron density for the COOH-terminal anionic region of GpIbα in the complex. This was unexpected, because this region affects rolling of GpIbα-expressing Chinese hamster ovary cells over VWF (*19*) but is consistent with our observation that the anionic region has no notable effect on binding to VWF-A1 (*16*).

The flexible loop from 227 to 241 in the COOH-terminal flank of GpIbα undergoes a conformational change on complex formation. In the complex, this loop, which we call the β switch, forms a 16-residue β hairpin that extends from residues 227 to 242 and aligns with the β3 strand of A1 (residues 562 to 566), forming a continuous β sheet shared between the two molecules (Fig. 1D). The gain-of-function mutations related to platelet-type von Willebrand disease are all found in the β switch. The specific mutation M239V that we used to obtain crystals of the complex enhances binding about threefold and is located in the β-switch strand that directly hydrogen-bonds to β3 of A1. Val^{239} provides two intermolecular main-chain hydrogen bonds, and its side chain contacts Tyr^{600} of helix α3 in A1. On the basis of the structure, similar interactions with methionine in the wild-type protein may be expected. Other known gain-of-function mutations include G233V, which like M239V is detected in patients with platelet-type von Willebrand disease (*20*, *21*); and V234G, D235V, and K237V, which were identified by site-directed mutagenesis (*14*, *15*). Four of the five gain-of-function mutations involve amino acid substitutions known to stabilize β-hairpin structures by introducing either a Cβ-branched residue in the strands (G233V, M239V, and K237V) or a glycine residue in the tight turn (V234G) (*22*). The mutation M239V increases the association rate threefold and hardly affects the dissociation rate, which is consistent with the stabilization of the β hairpin priming the mutant GpIbα for binding to A1. Unclear at this stage is how D235V, at the second position in the tight turn, induces β-hairpin formation and enhances the binding affinity. However, the locations of all five mutations support an indirect mechanism by influencing the conformation, because the side chains have either no or few direct contacts to A1 in the complex. Other valine substitutions in this region (K231V, Q232V, A238V, and T240V) that reduce binding affinity (*15*) may be explained in part by steric hindrance (Q232V and A238V) and by loss of a hydrogen bond with Asp^{560} of A1 (T240V). Overall, we conclude that the conformational equilibrium of the β switch of GpIbα is a critical factor in the precisely balanced affinity of the interacting partners.

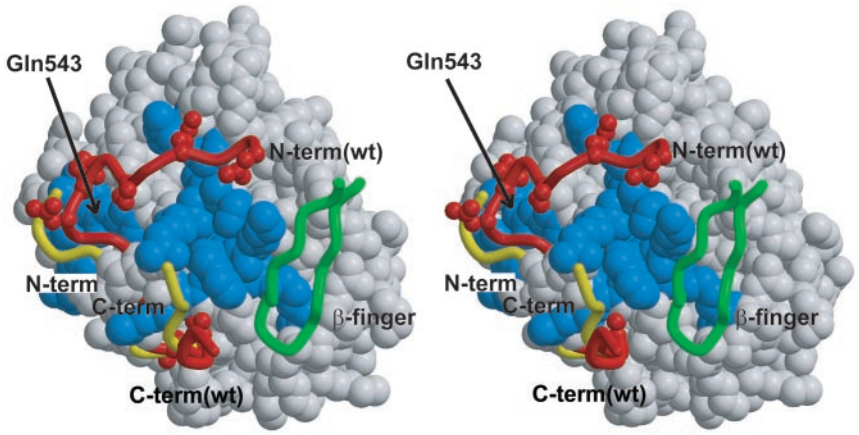

Fig. 2. Stereo representation of structural changes at the NH_2- and COOH-terminal side of VWF-A1. The bottom face of the A1 domain, as observed in the complex with GpIbα, is shown in space-filling representation with the NH_2- and COOH-terminal peptides shown as Cα-traces in yellow. The position of the β finger of GpIbα is given by a Cα-trace in green. The Cα-traces of the NH_2- and COOH-terminal peptides of the uncomplexed, wild-type (wt) A1 domain (*7*) are shown in red. Residues with known gain-of-function mutations yielding a type 2B von Willebrand disease phenotype are shown either in ball-and-stick representation in the wt NH_2- or COOH-terminal peptides or colored blue in the space-filling model of the bottom face. In full-length VWF, flanking peptides of A1 possibly shield the binding site of the β finger of GpIbα.

Table 1. Data collection and refinement statistics. Data were collected on beamline ID14-2 at the ESRF and on beamline X11 at the EMBL outstation [Deutsches Elektronen-Synchrotron (DESY)]. Data were processed with DENZO and SCALEPACK (*26*). Structures were solved in conjunction by molecular replacement. A model of A1 (*7*) was placed in the unit cell of the complex with CNS (*27*). Solvent flattening with CNS revealed β strands of GpIbα leucine-rich repeats. A mask was constructed around the putative GpIbα molecule, and the electron density inside the mask was used for molecular replacement with AMoRe (*28*). This identified two molecules in the asymmetric unit of the GpIbα crystal. Improved electron density obtained after density modification and phase extension to 2.5 Å was used for model building with O (*29*). The model was refined at 1.8 Å resolution with CNS and then used, with the model of A1 (*7*), as the starting point for refinement of the GpIbα-A1 complex. Refinement included bulk solvent correction and calculation of R_{free} with 5% of the reflections. The structures of GpIbα and the GpIbα-A1 complex have been deposited in the Protein Data Bank with ID numbers 1M0Z and 1M10, respectively.

	GpIbα (ESRF)	GpIbα-A1 (DESY)
	*Data collection statistics**	
Space group	*C2*	$P6_1$
Unit cell dimensions (Å, °)	a = 121.5, b = 54.5, c = 101.8, β = 103.7	$a = b$ = 89.8, c = 124.6
Resolution (Å)	40.0–1.85 (1.9–1.85)	40.0–3.1 (3.2–3.1)
Completeness (%)	97.8 (80.8)	99.9 (99.9)
Mosaicity (°)	0.4	0.2
Redundancy	3.6 (2.4)	5.8 (5.4)
R_{merge} (%)	7.3 (33.7)	8.7 (48.0)
I/σ_I	16.3 (2.9)	19.3 (3.6)
	Refinement statistics	
R_{factor} (%)	18.7	23.4
R_{free} (%)	21.7	29.6
No. of protein atoms	4115 (dimer)	3690
No. of waters	687	0
rmsd bonds (Å)	0.005	0.009
rmsd angles (°)	1.3	1.6

*Values in parentheses are for the highest resolution shell.

The gain-of-function mutations related to type 2B von Willebrand disease are clustered at the bottom face of A1 (Fig. 2), adjacent to the interaction site with the β finger of GpIbα. Type 2B mutation R543Q, which we used in the structure determination of the complex, is located 20 Å away from the interaction site. It causes a ~2.5-fold increase in binding affinity of the isolated A1 domain. However, the affinity of the wild-type A1 domain [K_d ~30 nM (*16*)] is already much higher than the affinity of multimeric VWF, for which we do not detect any binding up to a concentration of 150 nM. Similarly, other studies have indicated that the affinity depends on the length of the A1-containing VWF fragment used [see for example (*9*)]. Therefore, the A1 domain used for crystallization lacks key structural elements that suppress GpIbα binding in multimeric VWF. In the crystal structure of the wild-type A1 domain (*7*), the NH_2- and COOH-termini approach the β-finger interaction site (Fig. 2), suggesting that longer terminal peptides could shield the binding site of the β finger in multimeric VWF. Type 2B mutations are likely to destabilize a network of interactions observed between the bottom face of A1 and its terminal peptides in the wild-type A1 structure (*7*), thereby making the binding site accessible. In the complex, we indeed observed a displacement of the termini away from the interaction site and a partial disordering of the NH_2-terminus. In comparison, the homologous integrin I–type domains bind their ligands at a different site, and the large conformational changes observed on ligand binding in I-domains (*23*) do not occur in A1. The mechanism of affinity modulation in the A1 domain is therefore different from that of I-type domains and likely involves conformational changes at the NH_2- and COOH-termini. Shear stress may induce these changes in immobilized VWF, causing activation in the platelet adhesion process.

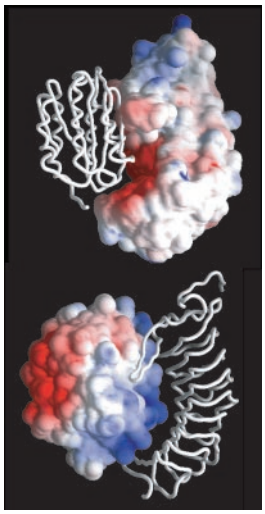

Fig. 3. Electrostatic surface potentials of the A1 domain of VWF and GpIbα. Potentials were calculated for the individual molecules. The surface is colored blue for potentials > 6 kT/e and red for potentials <−6 kT/e. The Cα-traces of the partner molecules in the complex are shown in white for clarity. The areas of large electrostatic potentials at the interface of A1 and GpIbα coincide with the region of loose, solvent-mediated contacts between the two molecules. Calculations were performed with GRASP (*30*).

The electrostatic surface potentials of GpIbα and A1 are characterized by large patches of opposite charge at the GpIbα-A1 interface that induce long-range electrostatic attraction (Fig. 3). In addition to the positively charged patch at the interface, A1 also shows a large negatively charged patch on the opposite side of the domain. Possibly, the asymmetric charge distribution on A1 helps to steer the long-range interactions. Crystal structures of P- and E-selectins, proteins that mediate rolling of leukocytes over inflamed endothelium, in complex with their ligands sialyl $Lewis^X$ or a sulfated peptide from PSGL-1 also indicated dominant electrostatic interactions (*24*). However, in the GpIbα-A1 complex, residues making up the charge potentials at the interface are not involved in direct contacts but are either fully or partially solvated. Thus, it appears that the surfaces of A1 and GpIbα are organized for long-range electrostatic attraction, avoiding the energetically unfavorable desolvation of charged residues (*25*) in the formation of the final complex.

The Bernard-Soulier syndrome and type 2M von Willebrand disease are characterized by loss-of-function mutations in GpIbα and VWF-A1, respectively. Loss-of-function mutations in the VWF-binding domain of GpIbα occur at buried sites (L57F, C65R, L129P, and A156V) or in a disulfide bond (C209S) and are likely to disturb the structural integrity of the domain, causing a reduction in binding affinity. Numerous loss-of-function mutations that were detected in von Willebrand disease type 2M patients (*8*) or identified by site-directed mutagenesis (*9–13*) are scattered throughout the A1 domain. Sixteen loss-of-function mutations involve residues in or directly next to the GpIbα-binding site, whereas 10 occur at buried positions inside the A1 domain and are likely to disrupt the A1 structure or to induce conformational changes to A1 that are incompatible with binding to GpIbα. The remaining 14 mutations are scattered over the surface outside the observed GpIbα-binding site, and their effects cannot be explained on the basis of the structure of the A1-GpIbα complex.

Our data suggest that GpIbα and VWF are attracted by long-range electrostatic interactions and indicate two contact sites in the final complex, which present primary targets for development of drugs for the treatment or prevention of arterial thrombosis. Interaction at the larger contact site depends on conformational changes in the β switch of GpIbα, whereas the second, smaller site most likely requires the dislodging of the termini of the A1 domain to uncover the site of interaction. Mutations that cause gain-of-function diseases favor the bound conformation at both contact sites. It is conceivable that under physiological conditions shear stress on immobilized VWF displaces the termini of the A1 domain, exposing the second binding site and hence enhancing platelet association to the site of vascular damage.

References and Notes

1. B. Savage, E. Saldívar, Z. M. Ruggeri, *Cell* **84**, 289 (1996).
2. S. Goto, D. R. Salomon, Y. Ikeda, Z. M. Ruggeri, *J. Biol. Chem.* **270**, 23352 (1995).
3. S. Goto, *Clin. Lab.* **47**, 327 (2001).
4. M. C. Berndt, Y. Shen, S. M. Dopheide, E. E. Gardiner, R. K. Andrews, *Thromb. Haemostasis* **86**, 178 (2001).
5. J. E. Sadler, *Annu. Rev. Biochem.* **67**, 395 (1998).
6. R. Celikel *et al.*, *Nature Struct. Biol.* **5**, 189 (1998).
7. J. Emsley, M. Cruz, R. Handin, R. Liddington, *J. Biol. Chem.* **273**, 10396 (1998).
8. D. Ginsburg, J. E. Sadler, *Thromb. Haemostasis* **69**, 177 (1993).
9. T. Matsushita, J. E. Sadler, *J. Biol. Chem.* **270**, 13406 (1995).
10. M. A. Cruz, T. G. Diacovo, J. Emsley, R. Liddington, R. I. Handin, *J. Biol. Chem.* **275**, 19098 (2000).
11. T. Matsushita, D. Meyer, J. E. Sadler, *J. Biol. Chem.* **275**, 11044 (2000).
12. S. Vasudevan *et al.*, *J. Biol. Chem.* **275**, 12763 (2000).
13. R. Celikel, Z. M. Ruggeri, K. I. Varughese, *Nature Struct. Biol.* **7**, 881 (2000).
14. A. S. Tait, S. L. Cranmer, S. P. Jackson, I. W. Dawes, B. H. Chong, *Blood* **98**, 1812 (2001).
15. J. Dong *et al.*, *J. Biol. Chem.* **275**, 27663 (2000).
16. Materials and methods are available as supporting material on *Science* Online.
17. B. Kobe, A. V. Kajava, *Curr. Opin. Struct. Biol.* **11**, 725 (2001).
18. A. Bateman *et al.*, *Nucleic Acids Res.* **30**, 276 (2002).
19. J. Dong *et al.*, *J. Biol. Chem.* **276**, 16690 (2001).
20. J. L. Miller, D. Cunningham, V. A. Lyle, C. N. Finch, *Proc. Natl. Acad. Sci. U.S.A.* **88**, 4761 (1991).
21. S. D. Russell, G. J. Roth, *Blood* **81**, 1787 (1993).
22. F. Blanco, M. Ramirez-Alvarado, L. Serrano, *Curr. Opin. Struct. Biol.* **8**, 107 (1998).
23. J. Emsley, C. G. Knight, R. W. Farndale, M. J. Barnes, R. C. Liddington, *Cell* **101**, 47 (2000).
24. W. S. Somers, J. Tang, G. D. Shaw, R. T. Camphausen, *Cell* **103**, 467 (2000).
25. F. B. Sheinerman, R. Norel, B. Honig, *Curr. Opin. Struct. Biol.* **10**, 153 (2000).
26. Z. Otwinowski, W. Minor, *Methods Enzymol.* **276**, 307 (1996).
27. A. T. Brünger *et al.*, *Acta Crystallogr.* **D54**, 905 (1998).
28. J. Navaza, *Acta Crystallogr.* **A50**, 157 (1994).
29. T. A. Jones, J. Y. Zou, S. J. Cowan, M. Kjeldgaard, *Acta Crystallogr.* **A47**, 110 (1991).
30. GRASP: Graphical Representation and Analysis of Surface Properties, 1993; A. Nicholls, Columbia University, New York.

31. We thank D. Westra and M. Bulsink for contributions to the early stages of the project, P. Lenting and E. Westein for technical assistance with Biacore measurements, H. Deckmyn (Kortrijk, Belgium) for supplying monoclonal antibody 2D4, and beamline scientists at the European Synchrotron Radiation Facility (ESRF) in Grenoble and at the European Molecular Biology Laboratory (EMBL) outstation in Hamburg for assistance during data collection. Supported by the "European Community–Access to Research Infrastructure Action of the Improving Human Potential Programme" to the EMBL Hamburg outstation, the Dutch Heart Foundation, and the Council of Medical Sciences of the Netherlands Organisation for Scientific Research.

Supporting Online Material

www.sciencemag.org/cgi/content/full/297/5584/1176/DC1

Materials and Methods

2 May 2002; accepted 20 June 2002